Biobased Polybenzoxazine Derived from Furfurylamine and Piceol with Low Cure Temperature and Advanced Properties for Composite Matrices

Michael J. Chauby*, Rocco P. Viggiano, Baochau N. Nguyen, Daniel A. Scheiman

M. Chauby, R. Viggiano

NASA Glenn Research Center, Cleveland, OH, 44135, USA

E-mail: michael.j.chauby@nasa.gov

B. Nguyen, D. Scheiman

Universities Space Research Association, 425 3rd Street SW, Suite 950, Washington, DC 20024, USA

Funding: This work was funded through the Transformational Tools and Technologies (TTT) program and Convergent Aeronautics Solution (CAS) program through the NASA Aerospace Research Mission Directorate (ARMD).

Keywords: Benzoxazine, Furan, Piceol

Abstract

A novel benzoxazine made from furfurylamine, paraformaldehyde, and piceol, Bz-FA-HA, is assessed for applications in fiber reinforced (FR) composites. Piceol is a biobased phenolic compound derived from the roots of Norwegian spruce trees and contains a methyl ketone group at the para position. Bz-FA-HA is a liquid at room temperature, has a viscosity of < 1 Pa.s at temperatures above 90 °C, and a T_{onset} of cure at 132 °C. The carbonyl is found to react with the furan ring, yielding a crosslinking reaction, when cured above 180 °C as indicated by differential scanning calorimetry and thermogravimetric analysis coupled with Fourier transform infrared spectroscopy. Poly(Bz-FA-HA) has a Tg > 350 °C, attributed to the crosslinking reaction. Furthermore, the storage modulus is > 3 GPa, regardless of cure temperature. Poly(Bz-FA-HA) has a char yield at 800 °C of 65.0 % (62.3 % at 1000 °C), and a T_{onset} of decomposition of 357 °C in nitrogen. The resulting carbon formed during pyrolysis shrinks during the carbonization reaction and scanning electron microscopy imaging shows a cross-section with micro cracks. The high processability, advanced mechanical properties, and exceptional char yield make it a promising candidate as the matrix for FR composites.

1. Introduction

Benzoxazine is a bicyclic heterocyclic monomer made up of a benzene ring bonded to an oxazine ring. Benzoxazine synthesis entails the reaction of a primary amine, formaldehyde, and a phenolic derivative in a 1:2:1 molar ratio and was first reported in 1944 by Holly and Cope.[1] Since their inception, a vast catalog of monomers has been synthesized from a large assortment of primary amines and phenolic derivatives.[2] Commercially available benzoxazine uses aniline, methylamine, or other petroleum-based amines.[3] The oxazine ring undergoes a ring opening reaction yielding a cation during polymerization and cationic electrophilic substitution forms a Mannich bridge at the benzene ring of a neighboring benzoxazine monomer. Research on the polymerization mechanism of aniline or other similar petroleum-based amine benzoxazines has shown that the ortho position of the benzene ring is preferable for the Mannich bridge as compared to the para position.[4] Polymerization of the benzoxazine monomer yields a polymer with superior properties compared to traditional phenolic resins, including a near zero volume shrinkage during cure, high glass transition temperature (Tg) and high char yields.[2]

The aromatic content in these resins is increased to improve their mechanical properties, glass transition temperature (T_g), and thermal stability. However, this sacrifices their processability especially when considering applications in fiber reinforced polymer (FRP) composites. Replacement of these petroleum-based amines with furfurylamine, a derivative of the renewable agriculture feedstock furfural, has gained significant attention in the last decade.[5] Furfurylamine is a furan-based amine that is readily prepared from renewable resources such as corn cobs.[6-8] Previous work in the literature has shown that replacing petroleum-based amines with furfurylamine increases the char yield.[9-12] These enhanced properties make furan-based polybenzoxazine exciting candidates as the polymer matrix precursor for carbon/carbon (C/C)-

composites expanding their applications to other FR composites. Researchers have developed difunctional furan-based benzoxazine from phenolic derivatives with multiple hydroxyls like bisphenol A and furfurylamine or from phenolic derivatives with a single hydroxyl and a difuran diamine (DFDA).[13-16] However successful in increasing thermal performance, these multifunctional materials again sacrifice processability for their superior properties. Therefore, maintaining superior properties while maintaining high processability is of great interest for further commercialization of benzoxazine.

Monofunctional petroleum-based benzoxazines are generally smaller molecules with respect to multifunctional materials making them more processable with respect to viscosity but with a single oxazine ring are unable to crosslink during polymerization.[3] This linear polymer topology increases their difficulty to cure and limits their commercial viability. Previous work in the literature suggests that the furan ring can participate in cationic electrophilic substitution reducing the temperature of cure compared to petroleum-based benzoxazine.[10,11,17-19] This gives exciting applicability to monofunctional furan-based benzoxazine in composite materials due to their reduced viscosity and increased processing window compared to multifunctional monomers.[9] Existing literature regarding these materials commonly uses phenol or biobased phenolic feedstocks.[10] This includes, but is not limited to guaiacol, eugenol, vanillin, cardanol, and sesamol.[11,20-25] Often, the focus of this work is regarding the synthesis of bio-based and renewable materials. However, these biobased phenolic derivatives mentioned have substituents at the -ortho and/or -para position on the phenol, which reverts to the original issue of difficulty in curing these materials. The substituents limit polymerization sites and cause difficulty in curing, a problem that also applies to monofunctional petroleum-based benzoxazine.

Yu first proposed that a furan-based benzoxazine monomer made using Gastrodigenin (4-hydroxybenzyl alcohol), Bz-FA-H, will form a cross-linked polymer network.[26] Gastrodigenin has a hydroxymethyl group substituent at the para position of the phenol that was shown to react with the furan ring in a crosslinking reaction at high temperatures of cure (> 220 °C). Expanding on this, previous work showed that furan ring not only participates in the polymerization of Poly(Bz-FA-H) but opens simultaneously during the crosslinking reaction where water is generated as a byproduct.[27] Furan conversion was measured using Fourier Transform Infrared (FTIR) spectroscopy and found that conversion was below 100 %. Therefore, two potential cross-linkages were proposed that considered both open and closed furan rings. It was noted that these are only two of many potential reactions, and no mechanism was explicitly proposed. Furthermore, this unique crosslinking reaction was not shown in any other monofunctional furan-based benzoxazine tested. To the knowledge of the authors, this crosslinking reaction in a furan-based monofunctional monomer has only been reported in Bz-FA-H.

With relation to properties, the crosslinking reaction increased thermal stability, char yield, and mechanical properties to a certain extent. In particular, it was found that room temperature storage modulus (E') increased with conversion of the crosslinking reaction up to approximately 30 %. Beyond 30 %, E' began to decrease due to embrittlement. This variability in mechanical properties with respect to crosslinking, temperature of post cure, is not desirable for the material when considering FRP composite aerospace applications where material properties must be maintained over a wide temperature range. Therefore, the development of a furan-based monofunctional benzoxazine monomer that replicates this crosslinking reaction but maintains mechanical properties at higher temperatures would be valuable for both FRP composites as well as the precursor matrix to C/C-composites.

This work presents a novel furan-based monomer synthesized from furfurylamine, paraformaldehyde, and 4-hydroxyacetophenone, piceol. Piceol is a biobased material derived from the roots of Norwegian spruce trees.[28] Piceol is a phenolic derivative with a methyl ketone in the -para position. It is hypothesized that the ketone-containing para substituent in piceol will react with the furan ring analogous to the crosslinking behavior previously observed in the Gastrodigenin-derived system, thereby enabling a high-temperature crosslinking reaction. If possible, then the furan-based piceol polybenzoxazine should have superior char yield and mechanical properties while maintaining processability. Synthesis of this novel monomer will first be presented. Then, the crosslinking reaction will be shown and its impact on the mechanical properties. Finally, the thermal stability will be explored and applicability as a polymer precursor for C/C-composites will be considered.

2. Methods

2.1 Materials

4′-Hydroxyacetophenone 99 % [CAS No.99-93-4] (purchased from Sigma Aldrich), Furfurylamine ≥ 99 % [CAS No.617-89-0] (purchased from Sigma Aldrich), Paraformaldehyde powder 95 % [CAS No.30525-89-4] (purchased from Sigma Aldrich), toluene ≥ 99.5 % ACS reagent (CAS No.: 108-88-3) (purchased from Sigma Aldrich), ethyl acetate ACS reagent ≥ 99.5 % (CAS No.: 141-78-6) (purchased from Sigma Aldrich), sodium hydroxide ≥ 98 % reagent grade pellets (anhydrous) (CAS No.: 1310-73-2) (purchased from Sigma Aldrich), magnesium sulfate

anhydrous free-flowing Redi-Dri™ ReagentPlus® ≥ 99. 5% (CAS No.: 7487-88-9) (purchased from Sigma Aldrich). All items were used as received.

2.2 Methods

Fourier transform infrared (FTIR) spectroscopy experiments were performed with a Nicolet IS50 FTIR spectrometer in absorbance mode with a diamond ATR crystal and a DLaTGS-KBr detector. Differential scanning calorimetry (DSC) experiments were performed with a TA Instruments X3DSC. Approximately 10 mg samples were loaded in hermetically sealed T-zero DSC pans and heated to 300 °C at 5 °C min^{-1} under a nitrogen atmosphere (50 mL min^{-1} flow rate). Thermogravimetric analysis (TGA) experiments were performed using a TA Instruments Q500. Approximately 5-15 mg of sample in a platinum pan heated at 10 °C min^{-1} from 50 - 1000 °C in a nitrogen atmosphere (60 mL min^{-1} balance flow rate and 40 mL min^{-1} sample flow rate). The initial decomposition temperature ($T_{5\%}$), or temperature when 5 wt.% has decomposed, and the final residual mass at 800 °C, char yield (CY_{TGA}), were recorded. Thermogravimetric analysis Fourier Transform Infrared (TGA-FTIR) spectroscopy experiments were performed using a TA Instruments Hi-Res TGA 2950 and a Nexus 470 FTIR with a mercury cadmium telluride (MCT) detector. Approximately 5 - 15 mg of sample in a platinum pan was heated at 20 °C min^{-1} from room temperature to 800 °C in a nitrogen atmosphere (40 mL min^{-1} balance flow rate and 20 mL min^{-1} sample flow rate) with the transfer line and FTIR gas cell temperature at 240 °C. Dynamic mechanical analysis (DMA) experiments were performed on a TA Instruments Q800 DMA in a single-cantilever mode with the oscillation frequency set to 1 Hz, the amplitude set to 10 μm, and temperature ramp rate of 2 °C min^{-1}. Pyrolysis of samples was done using a Lindberg 5463 hinged tube furnace. Approximately 15 x 15 x 3 mm samples weighing 3 grams were tested at 10 °C min^{-}

[1] from 25 - 1000 °C in an argon environment. A thermocouple probe was used inside the furnace directly above the sample to ensure accurate heating during testing. Pyrolyzed samples were evaluated for char yield (CY_{HTF}). The pyrolyzed samples were evaluated for volume change (ΔV). Volume change during carbonization was approximated using two methods. The first method ($\Delta V_{\Delta t}$) was found as the ratio of the difference in final thickness to initial thickness divided by the initial thickness as shown in **Equation 1**. The second method (ΔV_{tot}) was found as the ratio of the difference in polymer dimensions to carbon divided by the polymer as shown in **Equation 2**. The dimensions were measured using calipers.

$$\Delta V_{\Delta t} = \frac{t_{Carbon} - t_{Polymer}}{t_{Polymer}} \text{x } 100\ \% \quad (1)$$

$$\Delta V_{tot} = \frac{V_{Polymer} - V_{Carbon}}{V_{Polymer}} \text{x } 100\ \% \quad (2)$$

Scanning electron microscopy (SEM) was performed on a Hitachi S-4799-11 field emission scanning electron microscope using samples coated with gold/palladium. Raman spectroscopy was performed using a DXR Nicolet Raman Microscope equipped with a 633 nm laser was used for the experiments. The D-band or "defect-induced band" (~1360 cm^{-1} at 514 nm), the G-band or "graphite allowed-band" (~1560 cm^{-1} at 514 nm), and the 2D-band, which is an overtone of the D-band, (~2670 cm^{-1} at 514 nm) were only considered.[29] The ratio of the D/G bands and ratio of the 2D/G bands were found. X-ray diffraction (XRD) was performed with a Bruker D8 Discover with a Beryllium detector. Samples were crushed into powders using a mortar and pestle and tested from 10 to 90 ° 2-theta (2Θ) at 0.02 ° step size. The quantification characterization is done using the Wulff-Bragg formula to find the interplanar distance, d_{002} shown in **Equation 3**.[30,31] Here, Θ_{002} is the 002-plane peak position (radians), and λ is the wavelength

of the incident wave (λ = 1.5406 Å for X-rays). The Scherrer equation finds the crystalline height, L_c, in reference to the 002-plane and the crystalline diameter, L_a, in reference to the 10ℓ-plane shown in **Equation 4** and **Equation 5**, respectively.[30,32,33] Here, Θ_n is the 2-theta position of peak n (radians), λ is the wavelength of the incident wave (λ = 1.5406 Å for X-rays), and B_n is the full width at half maximum (FWHM) for peak n (radians).

$$d_{002} = \frac{\lambda}{2\sin\left(0.5 * \theta_{002}\right)} \tag{3}$$

$$L_C = \frac{0.89\lambda}{B_{002}cos\left(\theta_{002}\right)} \tag{4}$$

$$L_a = \frac{1.84\lambda}{B_{100}cos\left(\theta_{10\ell}\right)} \tag{5}$$

2.3 Synthesis of 4-hydroxyacetophenone Furan-Based Benzoxazine (Bz-FA-HA)

4-hydroxyacetophenone (68.1 g, 0.5 mol), furfurylamine (48.6 g, 0.5 mol), and paraformaldehyde (30 g, 1 mol) were charged to a 500 mL round bottom flask with approximately 50 mL of toluene and reacted at 85 °C for 6 hours under reflux. Approximately 400 mL of a 1:1 volume ratio of ethyl acetate to toluene was added to dilute the solution in preparation for purification washing steps. The solution was washed with 150 mL (x3) 2M NaOH (aq.) followed by 150 mL (x3) DI water. The solution was treated with $MgSO_4$ for 48 hours, filtered and rotary evaporated to remove the solvent. An overview of the synthesis reaction for the 4-hydroxyacetophenone furan-based benzoxazine (Bz-FA-FA) monomer is shown in **Figure** 1. A yield of 44 % was obtained with a purity of 95 % based on proton NMR (^{1}H NMR) and carbon NMR (^{13}C NMR). ^{1}H NMR (400 MHz, $CDCl_3$, ppm): 7.78 (dd, 1H, J=8.4, 1.8 Hz), 7.66 (dd, 1H, J=1.8, 0.4 Hz), 7.43 (dd, 1H, J=1.8, 1.1 Hz), 6.86 (dd, 1H, J=8.4, 0.4 Hz), 6.38 (dd, 1H, J=3.4,1.8 Hz), 6.28 (dd, 1H, J=3.4,1.1 Hz), 4.98 (d, 2H, J=6.7 Hz), 4.07 (2H, s), 3.93 (d, 2H, J=12.0 Hz),

2.55 (3H, s). ^{13}C NMR (400 MHz, CDCl3, ppm): 196.9 (1C, s), 158.6 (1C, s), 151.3 (1C, s), 143.2 (1C, s), 130.2 (1C, s), 128.8 (1C, s), 128.5 (1C, s), 119.4 (1C, s), 116.5 (1C, s), 110.4 (1C, s), 109.4 (1C, s), 82.6 (1C, s), 49.2 (1C, s), 48.3 (1C, s), 26.1 (1C, s). The ^{1}H and ^{13}C NMR are shown in the Supplemental Information **Figure S1** and **Figure S2**.

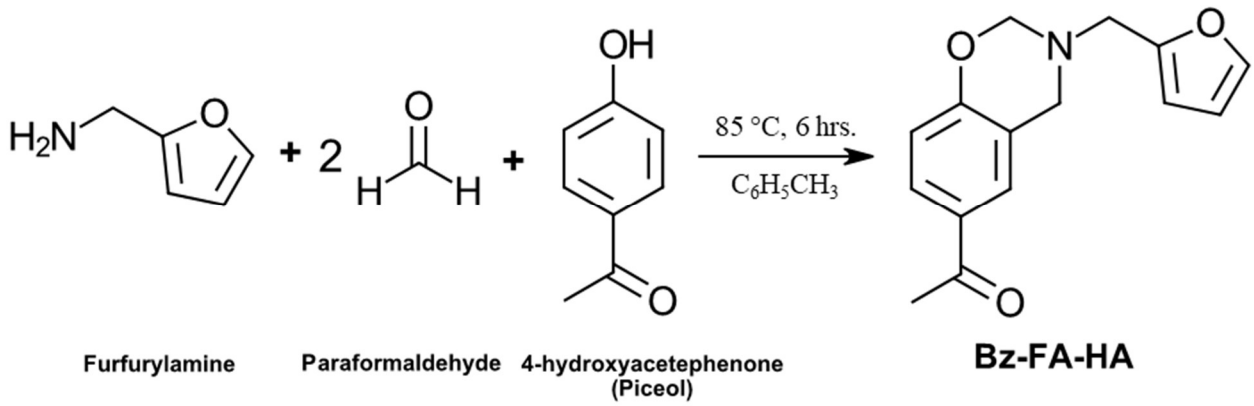

Figure 1. Synthesis overview of 4-hydroxyacetophenone furan-based benzoxazine (Bz-FA-HA) monomer

2.4. Poly(Bz-FA-HA) Cure

Bz-FA-HA monomer was heated to 90°C under vacuum for one hour to remove air trapped in the resin. The warm resin was then poured into molds and placed in an oven. The benzoxazine was cured using the following cure schedule: 130°C for 6 hours, 140°C for 1 hour, 150°C for 1 hour, 160°C for 1 hour, 170°C for 1 hour, 180°C for 1 hour, 200°C for 1 hour, 220°C for 1 hour, 240°C for 1 hour, and 260°C for 1 hour. In some instances, the polybenzoxazine was removed during the cure and analyzed to better understand the impact of temperature on material properties.

3. Discussion/Results

3.1 Properties of Bz-FA-HA Monomer and Polymerization

The cure cycle for Poly(Bz-FA-HA) was confirmed by the DSC curve of the benzoxazine monomer. The DSC curve is shown in **Figure 2**. The onset temperature of polymerization, T_{onset}, was 132 °C and the temperature of the peak exothermic polymerization reaction was 180 °C. The monomer had a T_g at approximately -15 °C, and no melting point indicating that it was a liquid at room temperature. A liquid state at room temperature makes this resin attractive as a matrix for FRP composites. However efficient and cost-effective processing is dependent on the viscosity of the monomer. The viscosity of the Bz-FA-HA monomer was assessed with respect to temperature and is reported in **Figure 3**. A viscosity of < 1 Pa.s was obtained at temperatures exceeding 90 °C. This provides a general window of high processability of approximately 40 °C, between 90 and 132 °C. The T_{onset} is considerably lower when compared to other furan-based benzoxazine monomers.

The polymerization exotherm is observed as a main narrow peak with a broad higher temperature “shoulder”. This indicates that two different reactions may be occurring during the polymerization. It is proposed that during the main exothermic reaction from the T_{onset} to the T_{peak} as shown in Figure 2 of the DSC curve, there is -ortho azine polymerization (OAP) and furan branching (FB) due to the oxazine ring opening. From previous work, the furan ring may also be opening simultaneously, but was not investigated in this work.[27] Beyond the T_{peak} of the main exotherm, an exothermic high temperature “shoulder” can be observed in the DSC curve in Figure 2. It is proposed that this high temperature shoulder represents a crosslinking reaction unique to Poly(Bz-FA-HA) and is onset when heated beyond 180 °C. These claims will be investigated in the next section using FTIR and TGA-FTIR.

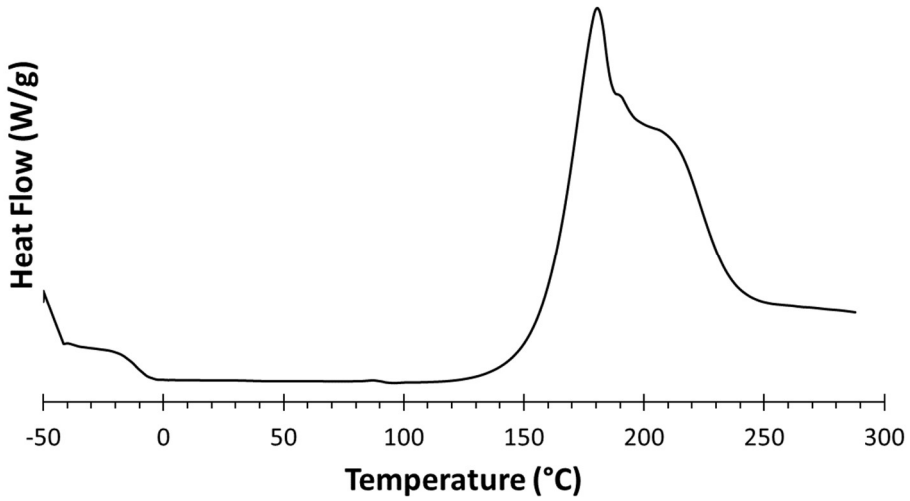

Figure 2. Differential Scanning Calorimetry (DSC) analysis of the polymerization cure behavior of Bz-FA-HA monomer

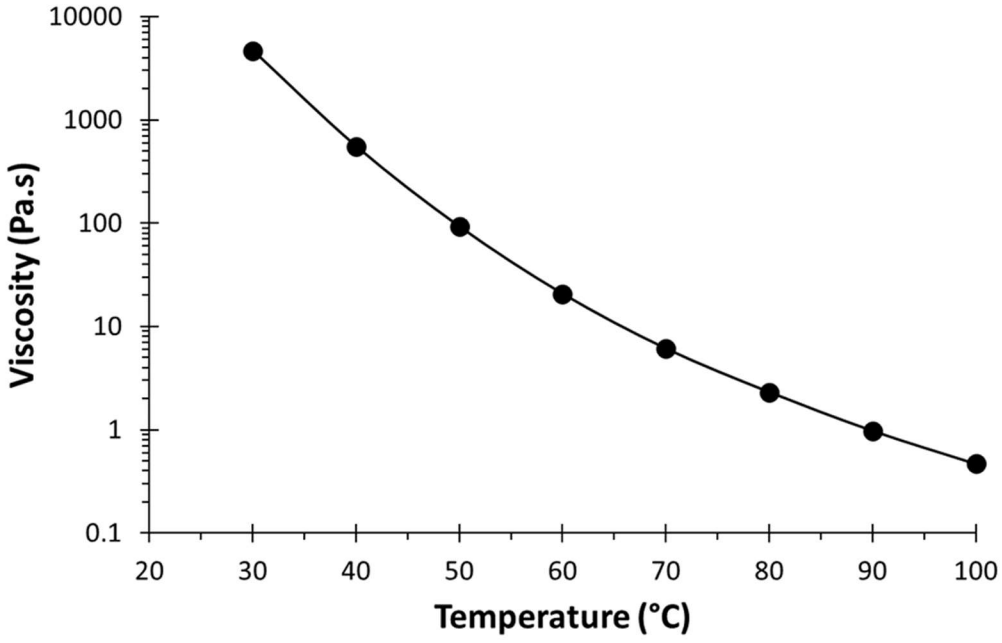

Figure 3. Viscosity analysis with respect to temperature of the Bz-FA-HA monomer

3.2 Poly(Bz-FA-HA) Polymer Network with Respect to Temperature

FTIR spectra were collected of the Poly(Bz-FA-HA) at various cure temperatures during its cure schedule. FTIR spectra for Poly(Bz-FA-HA) at 130 °C, 180 °C, 200 °C, and 260 °C are shown in **Figure 4**. There is a clear C=O peak at approximately 1670 cm^{-1} (labeled as A in Figure 4 insert). This peak was maintained throughout the whole cure cycle, indicating that if the ketone on the piceol participates in the crosslinking reaction, it is not fully consumed. Oxazine ring opening was monitored by the characteristic absorption peak of asymmetric stretching of the C-O-C at approximately 905 cm^{-1}.[13,17,34] The furan ring opening conversion is monitored by C-O-C stretching of the furan peak of the 1195 cm^{-1} peak and the branching by the 740 cm^{-1} peak representing the C-H stretching.[10,11,35]

At cure temperatures above 200 °C, the temperature of onset of the crosslinking reaction, there is broadening of the 1670 cm^{-1} peak, with a new shallow shoulder peak appearing at approximately 1705 cm^{-1} (labeled as B in Figure 4 insert). This would relate to the formation of a different type of C=O other than the one in piceol. This is believed to be the formation of the carbonyl from the furan ring opening.

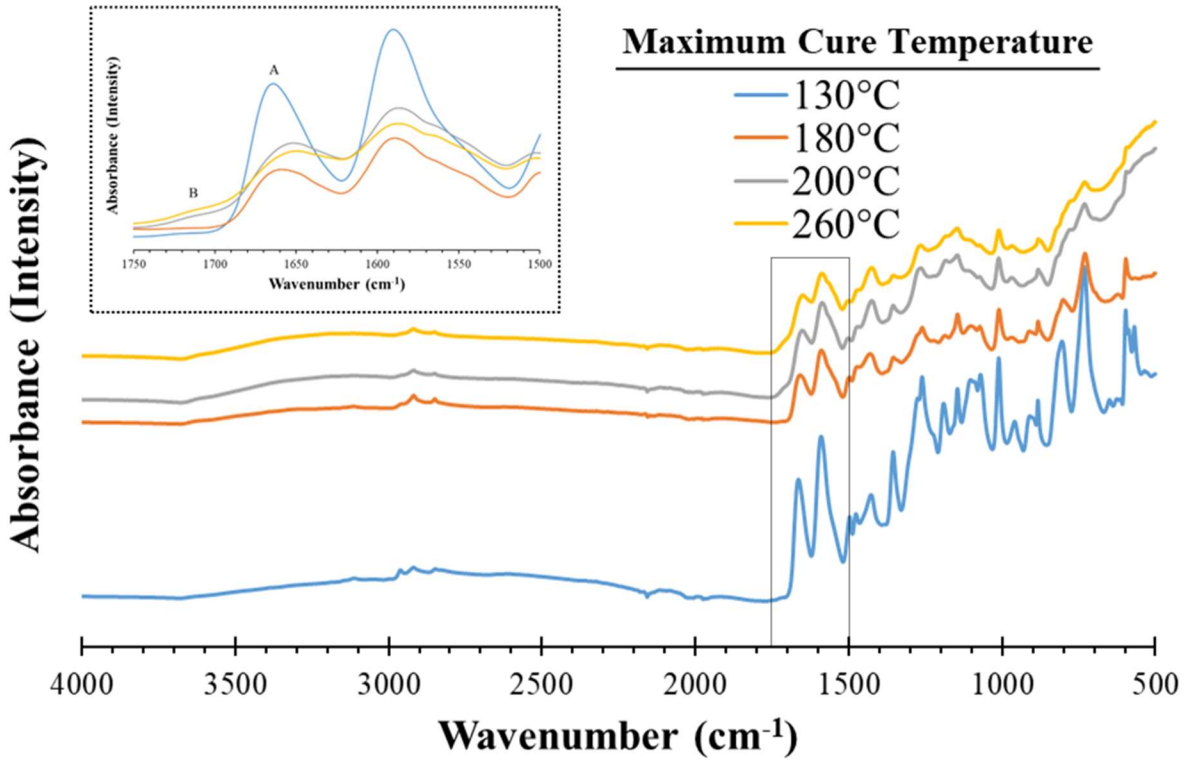

Figure 4. Fourier Transform Infrared (FTIR) spectra of Poly(Bz-FA-HA) at different maximum temperatures of cure

Thermogravimetric analysis Fourier Transform Infrared (TGA-FTIR) spectroscopy was used to assess the volatile products during the cure and the carbonization of Poly(Bz-FA-HA). Poly(Bz-FA-HA) samples were tested after each isothermal hold step along the cure cycle correlating to maximum cure temperatures of 130, 140, 150, 160, 170, 180, 200, 220, and 260 °C. **Figure 5** shows the residual weight versus temperature curve and the derivative weight versus temperature curve for each experiment.

An increase in decomposition temperature was correlated to an increase in maximum temperature of cure. The initial mass loss for Poly(Bz-FA-HA) cured to 130 °C was approximately

190 °C, while the initial mass loss for Poly(Bz-FA-HA) cured to 260 °C was approximately 300 °C. Furthermore, the presence of this mass loss during cure can be seen in a distinct derivative weight peak at approximately 200 °C, that disappears as the maximum temperature of cure is increased. The final residual weight at 700 °C also changes with the maximum temperature of cure, where increasing cure temperature correlates with increases in final residual weight. The shift in final residual weight is approximately equal to any mass loss during cure, indicating that the carbonization reaction is not impacted by the extent of cure. The residual weight of more than 60 % at 700 °C regardless of temperature of maximum cure is significant for polybenzoxazine materials, especially when considering feasibility for use as a precursor in carbon/carbon (C/C)-composites. A more robust study on thermal stability and the resulting carbon is presented in a future section.

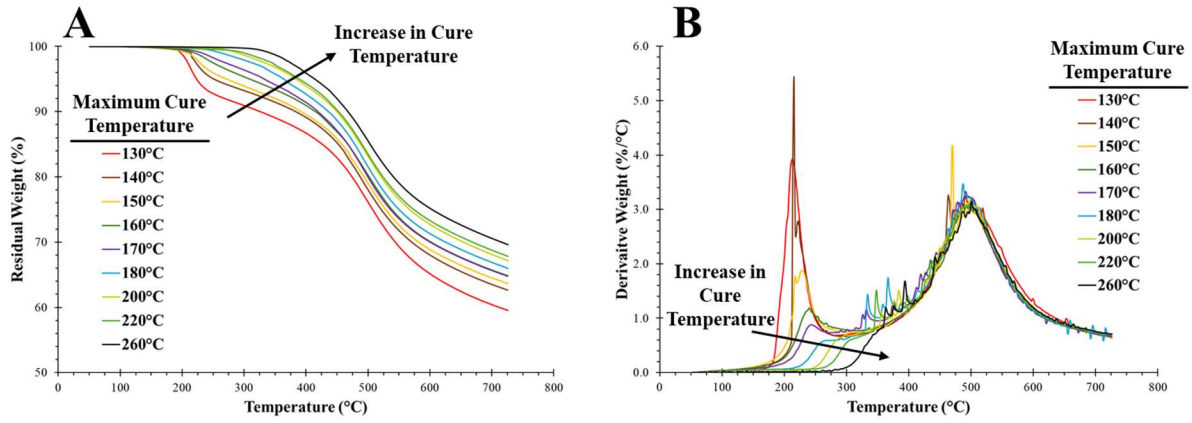

Figure 5. Thermogravimetric analysis (TGA) data of the carbonization of Poly(Bz-FA-HA) cured to 260°C and Bz-FA-HA monomer resin during stepwise cure cycle and carbonization

The FTIR spectra of volatile gases formed during TGA of Poly(Bz-FA-HA) is shown in Supplemental **Figure S3 – S7**. The only product present in the FTIR spectra at 200 °C is water. Therefore, the majority of the mass loss during the cure of Poly(Bz-FA-HA) can be attributed to water generation. However, we now know based on the TGA data in Figure 5 that the mass loss is

only present at above 190 °C, when the high temperature shoulder in the DSC curve shown in Figure 2 is onset. It can be deduced that this water generation, which causes mass loss during cure of the Poly(Bz-FA-HA), is a by-product of the proposed high temperature shoulder crosslinking reaction. This will be expanded upon in the next section.

Heating to 300 °C, water is still present, but carbon dioxide and/or carbon monoxide is generated as well. This correlates to the onset of the main carbonization reaction. The FTIR spectra at the temperature range from 400 to 700 °C, include water, carbon dioxide, carbon monoxide, aliphatic hydrocarbons (methane, ethane, etc.), aromatic hydrocarbons (benzene), and phenolics (phenol). These volatiles are a result of the main carbonization reaction and the products observed are consistent with typical polybenzoxazine precursors.[36]

With this understanding, a proposed polymer network of Poly(Bz-FA-HA) can now be considered. As previously hypothesized, the polymer topology of Poly(Bz-FA-HA) is proposed to change based on maximum temperature of cure. During the main exothermic reaction from the T_{onset} to the T_{peak} as shown in Figure 2 of the DSC curve, there is -ortho azine polymerization (OAP) and furan branching (FB) due to the oxazine ring opening generating a branched polymer topology. Furan branching would occur at the alpha carbon of the furan ring, since it can participate in the electrophilic substitution of the oxazine ring opening polymerization. Additionally, as determined using FTIR shown in Figure 4, at this temperature range there is a possibility for some of the furan rings to open during this exothermic polymerization. An alkoxide with a negative charge would be generated initially, but the most chemically stable form would be the generation of a ketone. At this temperature range, the furan ring can begin to open generating an alkoxide and then a more chemically stable ketone as determined using FTIR shown in Figure 4.

Figure 6 shows the most likely proposed branched polymer structure for Poly(Bz-FA-HA), where the ortho-azine polymerization (OAP) bonding is shown in blue and the furan branching (FB) is shown in green.

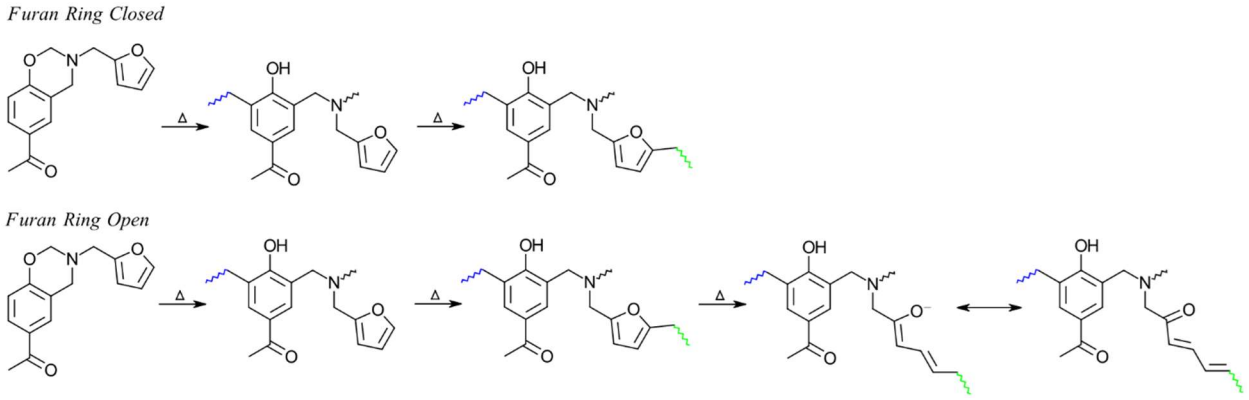

Figure 6. Proposed branched polymer topology of Poly(Bz-FA-HA) when cured below the temperature onset of the crosslinking reaction

Beyond the T_{peak} of the main exotherm, an exothermic high temperature "shoulder" can be observed in the DSC curve in Figure 2. It is proposed that this high temperature shoulder represents a crosslinking reaction unique to Poly(Bz-FA-HA) and is only onset when heated beyond 180 °C. Based on the TGA-FTIR data presented in Figure 5 and Supplemental Figure S3 – S7, there is a mass loss associated with this crosslinking reaction that pertains to water generation. With this understanding, two potential crosslinking structures will be proposed.

The most likely crosslinking reaction to consider is a condensation reaction between the carbonyl in the -para position of the benzene and closed furan rings that have not participated in branching. A condensation reaction with methyl ketones and furan rings to form anhydrotetramers was first reported by Ackman et al., and later confirmed by various others.[37-40] Although, this reaction was limited to methyl ketones in the presence of hydrochloric acid at temperatures of 100 °C, and not observed in ketones with aromatics such as acetophenone. With the increase in

temperature of the benzoxazine polymerization, combined with the anticipated increase in acidity from the oxazine ring opening, it is plausible to consider the feasibility that a condensation reaction between the carbonyl and two furan rings to create a crosslink. In this reaction, the carbon double bonded to the oxygen of the carbonyl bonds to the alpha carbon of two neighboring unopened furan rings, while the free hydrogen and the oxygen of the carbonyl generate water.

The second proposed crosslinking reaction would be an acetalization reaction between the alkoxide intermediate from furan ring openings and the carbonyl at the -para position of the benzene ring. The carbonyl is polarized, where the carbon atom has a partial positive charge, while the oxygen atom has a partial negative charge. When the furan rings open, they generate initially an alkoxide with a negative charge. The difference in polarity between the carbon on the carbonyl and the alkoxide could undergo an acetalization reaction to form first a hemiketal with one alkoxide and then a ketal with a second. **Figure 7** shows the two aforementioned proposed crosslinked structures of Poly(Bz-FA-HA), with OAP shown in blue, FB shown in green, the oxygen within the furan ring shown in pink, and the carbonyl oxygen of the piceol-derived methyl ketone group shown in red.

It should be noted that this is one of many potential reactions, included but not limited to Diels-Alder, keto-enol tautomerism, and/or a combination of these reactions. These potential crosslinking reactions will not be validated in this study, instead the claim that this crosslinking reaction is present will be explored. The mechanical properties with respect to temperature of cure before and after the proposed onset of the crosslinking reaction will be investigated in the next section. The limitation for the reactions presented is the steric hindrance of the aromatic on the carbonyl, and the need for either two unopened furan rings or two opened furan rings to one

carbonyl. However, this could cause limitations to the extent of crosslinking making a material with consistent properties over a wider temperature range and be consequentially beneficial to the material properties This idea will be explored in the next section with DMA.

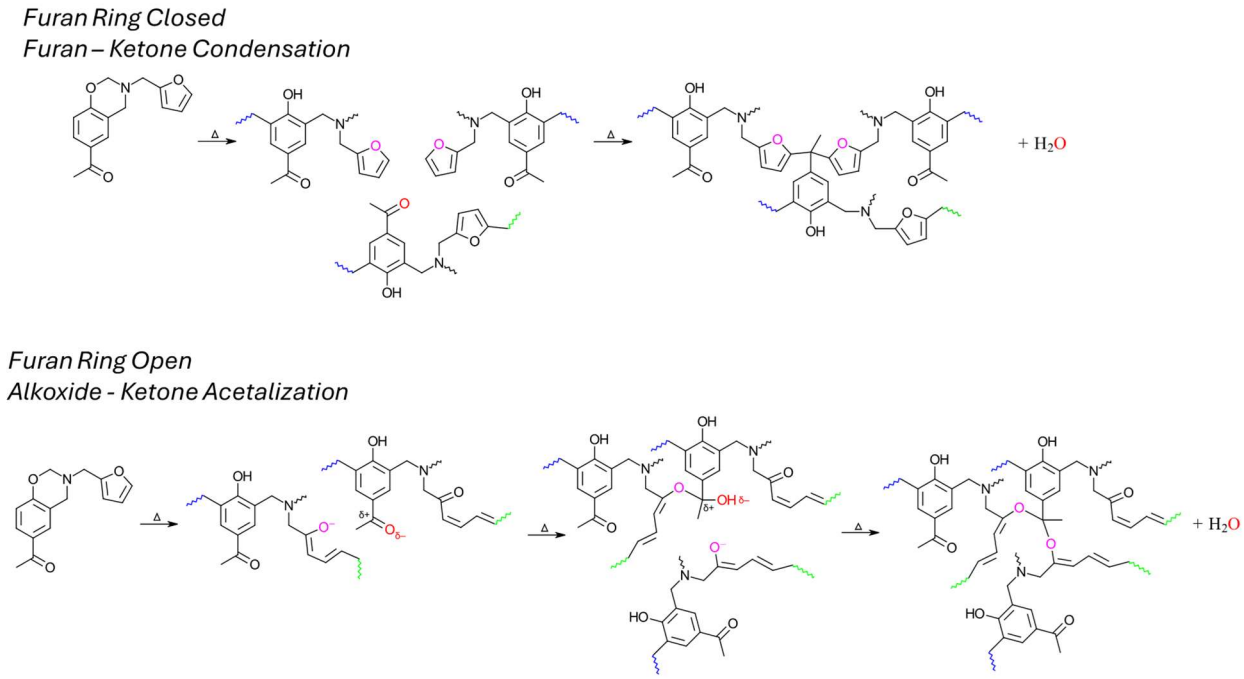

Figure 7. Proposed potential crosslinked polymer network of Poly(Bz-FA-HA) when cured above the temperature onset of the crosslinking reaction

3.3 Poly(Bz-FA-HA) Property Assessment with Respect to Temperature/Polymer Network

With a better understanding of how the polymer network of Poly(Bz-FA-HA) changes with respect to temperature, its impact on mechanical properties using DMA was assessed and used to verify the hypothesized crosslinking reaction. It is hypothesized that either the modulus and/or glass transition temperature (T_g) of the polymer would increase dramatically after heating beyond the onset of the crosslinking reaction. The storage modulus (E'), loss modulus (E"), and tan delta curves from DMA for Poly(Bz-FA-HA) cured to maximum temperatures of 180 °C, 200 °C, and

260 °C is shown in **Figure 8**. **Table 1** reports the E' at 25 °C and the T_g from both E" and Tan **δ**. At 180 °C, the maximum exothermic peak temperature was observed for the oxazine ring conversion with OAP and FB dominating polymerization, but with minimal to no onset of the crosslinking reaction. At 200 °C, the oxazine ring conversion associated with OAP and FB is complete, and the crosslinking reaction has begun and is near its maximum exothermic peak temperature. At 260 °C, the crosslinking reaction is complete as well. It is intended that these three temperatures would resemble the transition of the Poly(Bz-FA-HA) from its branched polymer topology to a crosslinked network.

The average storage modulus at 25 °C slightly decreased by approximately 11 %, while the T_g increased by more than 50 %, with respect to increased maximum temperature of cure. The highest E' value of 3.5 ± 0.5 was seen in Poly(Bz-FA-HA) cured to a maximum temperature of 180 °C, where the polymer topology was predominantly branched, while the lowest value of 3.1 ± 0.1 was seen when cured to a maximum temperature of 260 °C where the extent of the crosslinked polymer network is at its highest. This slight reduction however is within the standard deviation between the materials, which may indicate the presence of crosslinking, but indicates that the extent to which crosslinking is present in the material is not significant enough to embrittle the material and reduce its mechanical properties. A more effective confirmation for the presence of the crosslinking reaction can be seen in the significant increase in T_g. The highest T_g was 368 ± 6 observed in the Poly(Bz-FA-HA) cured to a maximum temperature of 260 °C where the extent of the crosslinking reaction is highest, while the lowest T_g was 209 ± 5 was observed when cured to a maximum temperature of 180 °C before the onset of the crosslinking reaction. The increase by more than 50 % provides preliminary validation that a significant change in polymer topology is observed in this temperature range, most likely a crosslinking reaction as previously presented.

Furthermore, the material's T_g exceeding 350 °C while maintaining a storage modulus greater than 3 GPa over a wide temperature range of maximum cure is a promising indication of its use in mechanically strong fiber reinforced composites.

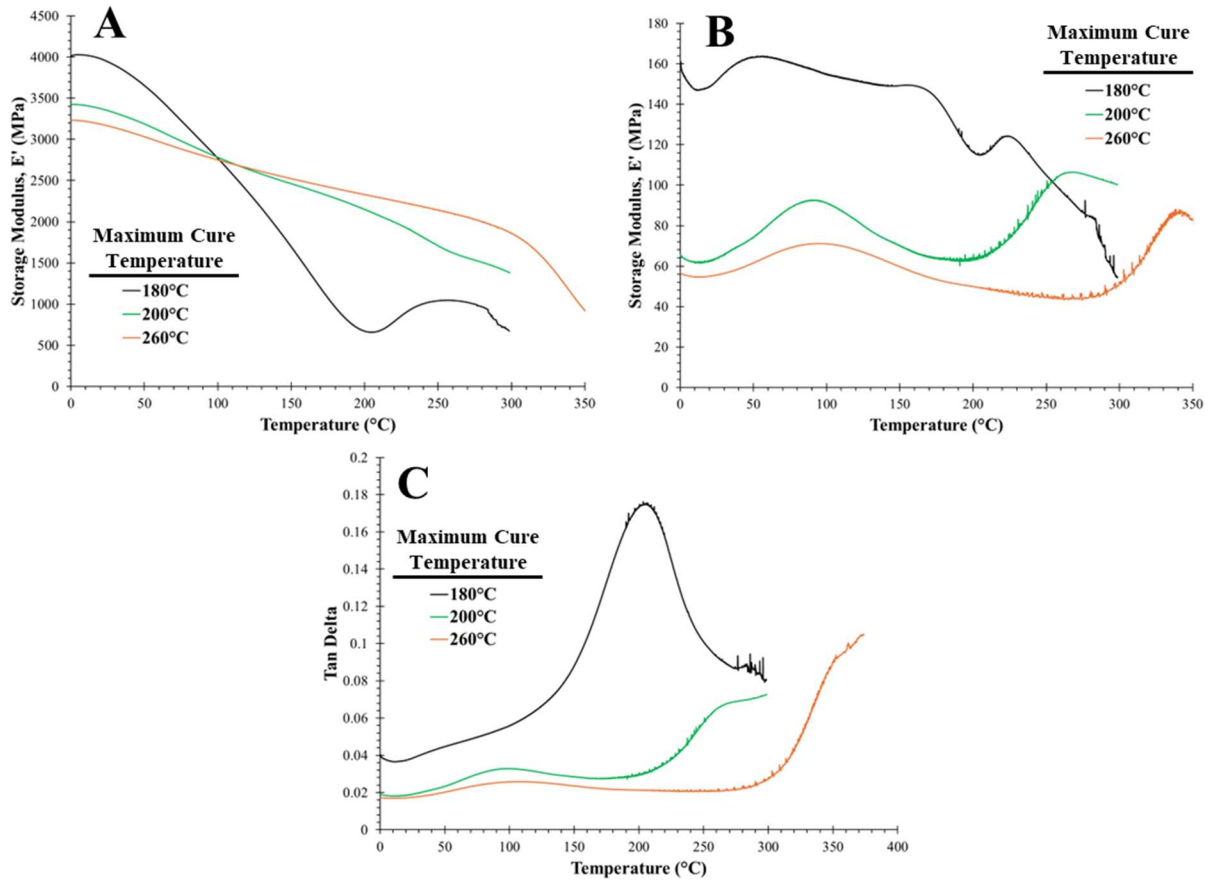

Figure 8. Dynamic mechanical analysis (DMA) data of Poly(Bz-FA-HA) cured to 180 °C, 200 °C, and 260 °C separated into A) Storage modulus, E', B) loss modulus, E", C) tan delta

Table 1. Dynamic mechanical analysis (DMA) data of Poly(Bz-FA-HA) cured to 180 °C, 200 °C, and 260 °C

Maximum Cure Temperature (°C)	Storage Modulus, E' @ 25°C (GPa)	Tg from E" (°C)	Tg from Tan δ (°C)
180	3.5 ± 0.5	226 ± 4	209 ± 5
200	3.2 ± 0.2	262 ± 9	266 ± 8
260	3.1 ± 0.1	343 ± 1	368 ± 6

3.4 Thermal Stability and Carbon Formation

The thermal stability of Poly(Bz-FA-HA) was briefly touched on when developing the understanding of volatile gases generated during both cure and carbonization through TGA-FTIR in Figure 5. A more detailed assessment of thermal stability will be presented in this section. The thermal stability of the fully cured Poly(Bz-FA-HA) (cured to a maximum temperature of 260 °C) and of the Bz-FA-HA monomer were assessed using TGA. The different materials allow for tracking residual weight with respect to temperature during carbonization with the initially fully cured polymer and the weight with respect to temperature during both cure and carbonization of the initial monomer. The char yield of the initial monomer is referenced as the effective char yield. The effective char yield quantitatively defines the entire weight loss of the material and unifies char yields for polymers whose char yield is impacted by temperature of cure. It is an important parameter when considering the feasibility of the polymer as a precursor for carbon/carbon (C/C)-composites. The Bz-FA-HA monomer was cured with the same cure cycle before heating to onset decomposition. The TGA curve can be seen in **Figure 9**.

The Bz-FA-HA monomer retained 80.4 ± 4.5 % of its initial weight after curing to a maximum temperature of 260 °C. After the cure cycle, the decomposition of the initial monomer followed the same decomposition curve as the initially fully cured polymer. The final char yield at 800 °C for the initial monomer, effective char yield, was 52.2 ± 3.2 %, while the initially fully cured polymer was 65.0 ± 0.5 %. The char yield reported for the material is significantly high when compared to other polybenzoxazine, and especially when considering other biobased polybenzoxazine. The T_{onset} of decomposition for Poly(Bz-FA-HA) was 357 ± 4 °C, lending to a high thermally stable material.

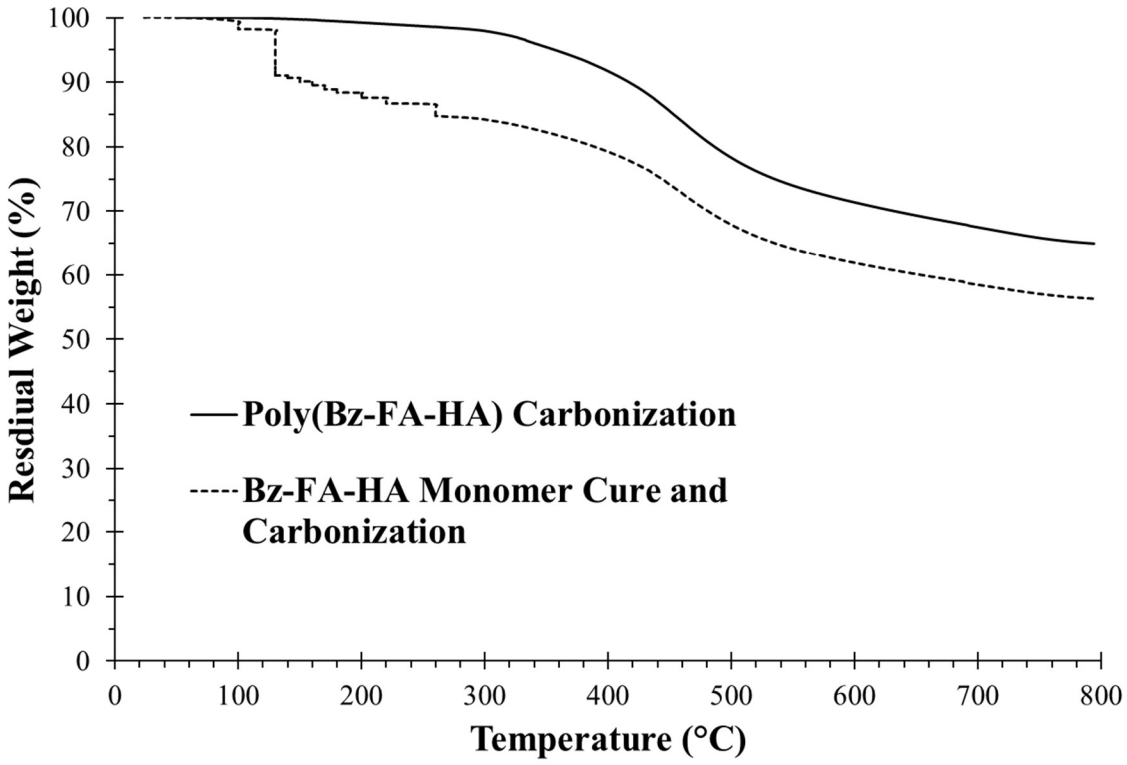

Figure 9. Thermogravimetric analysis (TGA) data of the carbonization of Poly(Bz-FA-HA) cured to 260°C and Bz-FA-HA monomer resin during stepwise cure cycle and carbonization

The high char yield reported indicates a potential feasibility for Poly(Bz-FA-HA) as a promising precursor matrix in the fabrication of C/C-composites. However, the resulting carbon generated must be assessed as well. The carbonization of Poly(Bz-FA-HA) was repeated using a hinged tube furnace (HTF). This allowed for validation of the char yields from TGA, as well as fabrication of larger quantity of carbon to better assess microstructure and density of resulting carbon. The char yield at 1000 °C from the HTF of Poly(Bz-FA-HA) was 62.3 ± 0.7 %. The slight reduction in char yield from the TGA experiment is attributed to the carbonization progressing to 1000 °C in the HTF, and only 800 °C in the TGA. The resulting carbon experienced a negative volume change during carbonization, also referred to volume shrinkage. With respect to thickness, the dimensional change was -15.2 ± 1.4 %, and with respect to overall volume, the dimensional

change was -44.3 ± 0.8 %. This shrinkage during carbonization is important with considering how interlaminar and trans tow cracks propagate through the material when shrinking as the matrix in fiber reinforcement.[41,42]

SEM was performed to assess the porous microstructure of the carbon during the volume shrinkage. SEM imaging of the carbon cross section is shown in **Figure 10**. The image shows cracks that were generated from the shrinkage of the material during the carbonization reaction. The cracks are mostly interconnected and predominately oriented through the thickness of the material, in other words, point towards the closest surface of the carbon. In addition to the larger cracks, there are smaller regions of porosity on the order of magnitude of 10 μm or smaller and are closed to the surface. The bulk density of the carbon was 1.38 ± 0.02 g cm^{-3}, which was an 11 % increase compared to the bulk density of the Poly(Bz-FA-HA) precursor of 1.24 ± 0.02 g cm^{-3}. The increase in bulk density is attributed to the higher skeletal density of the carbon backbone compared to the polybenzoxazine precursor backbone. It is important to note, that although skeletal density was not measured in this study, the change is large enough to offset the porosity observed in the cross section of the material.

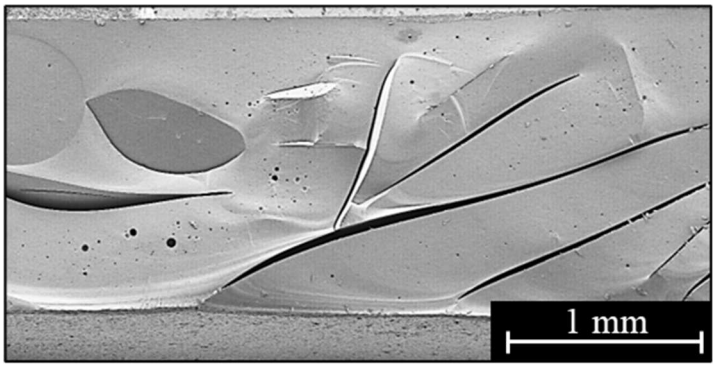

Figure 10. Scanning electron microscope (SEM) image of the carbon cross section from the carbonization of Poly(Bz-FA-HA) precursor

Raman spectroscopy and X-ray diffraction (XRD) are commonly used to characterize carbon structure. Raman spectroscopy is useful in determining the molecular arrangement of the carbon structure, while XRD can provide detailed information on the crystalline structure. The Raman spectra and XRD pattern are shown in supplemental **Figure S8** and **Figure S9**, respectively. The quantitative characterization from the analysis is reported in **Table 2**.

The Raman spectra show a distinct D-band or "defect-induced band" at ~1340 cm^{-1} and G-band or "graphite allowed-band" at ~1605 cm^{-1}. In perfectly ordered graphene, the D-band is absent and only becomes active in disordered carbon. Therefore, the presence of the D-band indicates that the carbon generated is not graphitizable, and common for carbon from thermosetting polymer precursors.[43,44] Comparing the ratio of intensities of the D to G ($\frac{I_D}{I_G}$) band can indicate whether the carbon is more ordered or disordered. Decreasing the intensity of the D to G band results in more ordered carbon with fewer defects. The D/G band ratio is 1.14 ± 0.03, indicating the presence of disordered non-graphitizable molecular structure.

A broad shallow 2D peak is present at ~2640 cm^{-1}, with likely contribution from other second order bands. A distinct 2D peak with no additional peaks would indicate the presence of monolayer graphene. As graphene begins to stack into multi-layer graphene, the material approaches highly ordered graphitic carbon. In graphitic carbon, the 2D band separates into $2D_1$ and $2D_2$ bands, which are reported at ~2670 cm^{-1} and ~2720 cm^{-1} for a 514 nm laser, respectively. The $2D_2$ band in graphitic carbon has an increased intensity when compared to the $2D_1$ band.[45] Due to the temperatures applied in this study, no graphitic carbon is believed to be generated, and therefore the $2D_2$ band is not evaluated and instead the $2D_1$ will be referred to as the 2D band for clarity. The ratio of the intensities of the 2D to G ($\frac{I_{2D}}{I_G}$) band can indicate whether the carbon

generated is similar to graphene, where increased intensity would be more similar.[46] The 2D/G band ratio is 0.18 ± 0.01, indicating the carbon formed is dissimilar to graphene and confirms the non-graphitizable nature of the material.

The XRD pattern shows a broad 002 plane peak between 18 - 30 ˚ and a broad 10ℓ plane peak between 40 – 47 °, which is found in carbon that has crystalline properties, but not graphitic. In non-graphitizable carbon, the 10ℓ plane does not have the three-dimensional diffraction lines as in graphitic carbon where distinct 100 and 101 plane peaks are observed.[31,32] The broad asymmetric 002 band is attributed in literature to the presence of saturated structures. It suggests the existence of another band at the lower scattering angle with overlapping intensities.[47] To accommodate this, the Wullf-Bragg formula was used to separate these intensities to more accurately report the interplanar distance. The d_{002} interplanar distance, d-spacing, of the carbon is 3.60 ± 0.02 Å, confirming the highly amorphous nature of the material. For reference, the d_{oo2} values for graphite is 3.392 Å, for carbon nanotubes is 3.442 Å, and turbostratic graphite is 3.44 Å.[48] The crystalline height, L_c, and the crystalline diameter, L_a, for the carbon is 13.8 ± 0.2 Å and 47.7 ± 0.9 Å, respectively.

Table 2. Molecular and crystalline structure of carbon from pyrolysis of Poly(Bz-FA-HA) precursor

$\frac{I_D}{I_G}$	$\frac{I_{2D}}{I_G}$	d_{002} (Å)	L_C (Å)	L_A (Å)
1.14 ± 0.03	0.18 ± 0.01	3.60 ± 0.02	13.8 ± 0.2	47.7 ± 0.9

When considering applicability for a polymer precursor to C/C-composites, the same initial principles apply as for fabricating FRP composites. Low monomer viscosity and low temperature of cure are important for not only processing of the initial FRP composite, but for infiltration of additional resin into the porous carbon matrix after pyrolysis to increase density. The iterations of infiltration and pyrolysis for thermosetting resins is commonly referred to as polymer infiltration and pyrolysis (PIP). PIP processing uses repeated polymer infiltration and pyrolysis cycling to achieve high density. The initial carbon fiber reinforced polymer (CFRP) composite fabrication is considered the first polymer infiltration step, where the first pyrolysis step would generate the initial C/C-composite.

The pyrolysis of the initial CFRP composite yields a porous network as a result of the volume change during carbonization and the mass loss of the polymer matrix precursor. The porous network is formed throughout the composite when the force of the volatile gases being formed and matrix volume change mechanism rupture the matrix and fiber-matrix interfaces. Porosity in a C/C-composite can be categorized as interlaminar cracks, trans tow cracks, and dry zones.[40,41,49,50] Porosity can be characterized as both open and closed. In closed porosity, the pores are inaccessible to the outside environment reducing the capacity for densification. In open porosity, the porosity is accessible to the outside environment and can be densified in pressure assisted densification processes. To ensure complete densification and no unwanted closed porosity, high pressure is typically used, but a resin with low viscosity can reduce the pressure to achieve complete infiltration therefore simplifying processing.

In addition, carbon properties must be considered. The overall volume shrinkage, and resulting bulk density, dictates the type of porosity generated and conversely the ability to densify

the C/C-composite. Dry zones are matrix regions composed of large voids; they are the result of volatile gas diffusion during pyrolysis. Trans-tow and interfacial cracks form parallel to the fiber tows and between layers, respectively and are caused by matrix volume change. Increasing the amount of shrinkage experienced during pyrolysis would increase the extent of cracks compared to dry zones, where cracks can be interconnected increasing open porosity and allow for complete densification. Therefore, the overall volume shrinkage during carbonization of Poly(Bz-FA-HA) is an indicator of its feasibility as a precursor material to C/C-composite.

Char yield of the precursor polymer is important because increased char yield will translate to higher amount of carbon initially after the first pyrolysis as well as subsequent infiltration steps. Therefore, having high char yield reduces processing time by reducing the amount of PIP steps needed to achieve complete densification, where complete densification is defined as the bulk density after pyrolysis is within 1% of the previous cycle.

Lastly, the type of carbon being formed should be considered. As previously stated, the carbon generated from the pyrolysis of Poly(Bz-FA-HA) is disordered, amorphous, and non-graphitizable. The carbon generated is not optimal for achieving high density and a mechanically robust material. However, this issue is not exclusive to Poly(Bz-FA-HA) and is common for carbon generated from thermosetting polymer precursors.

4. Conclusions

This study synthesized a novel monofunctional furan-based benzoxazine from paraformaldehyde, furfurylamine, and piceol, Bz-FA-HA. The monomer resin was shown to be a liquid at room temperature with a processable viscosity at temperatures above 90 °C and a low

temperature of cure at 130 °C. The polymerization of Poly(Bz-FA-HA) contained a primary main temperature exotherm with a maximum peak at 180 °C, as well as a high temperature shoulder at 200 °C. This high temperature shoulder was shown to be a result of a crosslinking reaction, and when Poly(Bz-FA-HA) was cured beyond it, the T_g of the material significantly increased from approximately 200 °C to more than 350 °C, while maintaining a modulus of >3 GPA. The thermal decomposition of the material was similar to the T_g of the material. The combined mechanical strength, high operation temperature, low monomer viscosity, and low temperature of cure provide great opportunity for these materials to be used as the polymer matrix in FRP composites.

Carbon from the pyrolysis of Poly(Bz-FA-HA) was fabricated and assessed for feasibility as the matrix material in C/C-composites. The char yield of Poly(Bz-FA-HA) at 800 °C was 65.0 ± 0.5 % by TGA and 62.3 ± 0.7 % at 1000 °C by HTF. The carbon experienced a negative volume change, volume shrinkage, during carbonization causing an increase in bulk density from 1.24 ± 0.02 g cm^{-3} of the Poly(Bz-FA-HA) to 1.38 ± 0.02 g cm^{-3} for the carbon. Cross sectional imaging from SEM showed that the volume shrinkage generated microcracks. The molecular and crystalline structure showed that the carbon generated was highly disordered and non-graphitizable carbon, which is common for thermosetting polymers. In comparison to other thermosetting polymers, Poly(Bz-FA-HA) has high char yield and experiences volume shrinkage during carbonization. These conditions are favorable in reducing costs when considering processing of C/C-composites through repeated cycling of infiltration and pyrolysis, also known as PIP processing.

The advanced Bz-FA-HA monomer properties, Poly(Bz-FA-HA) polymer properties, and resulting carbon properties after pyrolysis presented in this work demonstrate the viability of this

material as the matrix in both FRP composites and C/C-composites, both of which have numerous applications in both aeronautics and aerospace.

Acknowledgements

We would like to acknowledge financial support of the NASA Aeronautics Research Mission Directorate (ARMD) under the Convergent Aeronautics Solutions (CAS) program and the Transformational Tools and Technologies (TTT) program. The views and conclusions contained in this document are those of the authors and should not be interpreted as representing the official policies, either expressed or implied, of the U.S. government. The U.S. Government is authorized to reproduce and distribute reprints for Government purposes notwithstanding any copyright notation herein. Additionally, we thank Linda McCorkle (Universities Space Research Association) for SEM images and Dr. Yi Lin (NASA Langley Research Center) for the NMR testing.

Supporting Information

Supporting Information is available from the Wiley Online Library or from the author.

References

1. F. W. Holly and A. C. Cope, "Condensation Products of Aldehydes and Ketones with o-Aminobenzyl Alcohol and o-Hydroxybenzylamine," *Journal of the American Chemical Society* 66 (1944): 1875-1879. https://doi.org/10.1021/ja01239a022.

2. H. Ishida 2011. "Chapter 1 - Overview and historical background of polybenzoxazine research." in *Handbook of Benzoxazine Resins*. Edited by H. Ishida and T. Agag, Elsevier: ISBN 9780444537904.

3. S. Rimdusit, C. Jubsilp, and S. Tiptipakorn 2013. “Introduction to Commercial Benzoxazine and Their Unique Properties.” in *Alloys and Composites of Polybenzoxazines*. Springer: ISBN 978-981-4451-75-8.

4. C. Jubsilp, T. Takeichi, and S. Rimdusit 2011. “Chapter 7 - Polymerization Kinetics. Handbook of Benzoxazine Resins.” in *Handbook of Benzoxazine Resins*. Edited by H. Ishida and T. Agag, Elsevier: ISBN 9780444537904.

5. Y. Lyu and H. Ishida, “Natural-sourced benzoxazine resins, homopolymers, blends and composites: A review of their synthesis, manufacturing and applications,” *Progress in Polymer Science* 99 (2019): 101168. https://doi.org/10.1016/j.progpolymsci.2019.101168.

6. A. Gandini, T. M. Lacerda, A. J. F. Carvalho, et al., “Progress of Polymers from Renewable Resources: Furans, Vegetable Oils, and Polysaccharides,” *Chemical Reviews* 116, no. 3 (2016): 1637–1669. doi:10.1021/acs.chemrev.5b00264.

7. P. Zhang, X. Liao, C. Ma, et al., “Chemoenzymatic Conversion of Corncob to Furfurylamine via Tandem Catalysis with Tin-Based Solid Acid and Transaminase Biocatalyst,” *ACS Sustainable Chemistry & Engineering* 7, no. 21 (2019): 17636–17642. https://doi.org/10.1021/acssuschemeng.9b03510.

8. S. Jiang, W. Ramdani, E. Muller, et al., “Direct Catalytic Conversion of Furfural to Furan-derived Amines in the Presence of Ru-based Catalyst,” *ChemSusChem* 13, no. 7 (2020): 1699–1704. https://doi.org/10.1002/cssc.202000003.

9. Y. X. Wang and H. Ishida, “Development of low-viscosity benzoxazine resins and their polymers,” *Journal of Applied Polymer Science* 86, no. 12 (2002): 2953–2966. https://doi.org/10.1002/app.11190.

10. Y. L. Liu, and C. I. Chou, “High performance benzoxazine monomers and polymers containing furan groups,” *Journal of Polymer Science Part A: Polymer Chemistry* 43, no. 21 (2005): 5267–5282. https://doi.org/10.1002/pola.21023.

11. J. Wang, W. Liu, and T. Feng 2017. “Chapter 28 - Furan-Based Benzoxazines.” in *Advanced and Emerging Polybenzoxazine Science and Technology*. Edited by H. Ishida and P. Froimowicz, Elsevier: ISBN 9780128041703.

12. B. Lochab, M. Monisha, N. Amarnath, et al., “Review on the Accelerated and Low-Temperature Polymerization of Benzoxazine Resins: Addition Polymerizable Sustainable Polymers,” *Polymers* 13, no. 8 (2021): 1260. https://doi.org/10.3390/polym13081260.

13. R. Yang, M. Han, B. Hao, et al., “Biobased high-performance tri-furan functional bis-benzoxazine resin derived from renewable guaiacol, furfural and furfurylamine,” *European Polymer Journal* 131 (2020): 109706. https://doi.org/10.1016/j.eurpolymj.2020.109706.

14. M. Yu, S. K. Yadav, J. J. La Scala, et al., "Bio-based benzoxazine monomers and polymers based on difuran diamine," *Journal of Applied Polymer Science* 139, no. 39 (2022): 52946. https://doi.org/10.1002/app.52946.

15. X. Shen, J. Dai, Y. Liu, et al., "Synthesis of high performance polybenzoxazine networks from bio-based furfurylamine: Furan vs benzene ring," *Polymer* 122 (2017): 258–269. https://doi.org/10.1016/j.polymer.2017.06.075.

16. X. Wang, H. Niu, J. Huang, et al., "A desoxyanisoin- and furfurylamine-derived high-performance benzoxazine thermoset with high glass transition temperature and excellent anti-flammability," *Polymer Degradation and Stability* 189 (2021): 109604. https://doi.org/10.1016/j.polymdegradstab.2021.109604.

17. P. Thirukumaran, A. Shakila Parveen A, and M. Sarojadevi, "Synthesis and Copolymerization of Fully Biobased Benzoxazines from Renewable Resources," *ACS Sustainable Chemistry & Engineering* 2, no. 12 (2014): 2790–2801. https://doi.org/10.1021/sc500548c.

18. S. F. Li, "Synthesis of benzoxazine-based phenolic resin containing furan groups," *Chinese Chemical Letters* 21, no. 7 (2010): 868–871. https://doi.org/10.1016/j.cclet.2010.01.007.

19. C. Wang, J. Sun, X. Liu, et al., "Synthesis and copolymerization of fully bio-based benzoxazines from guaiacol, furfurylamine and stearylamine," *Green Chemistry* 10 (2012): 2799-2806. https://doi.org/10.1039/c2gc35796h.

20. W. Yang, H. Ding, D. Puglia, et al., "Bio-renewable polymers based on lignin-derived phenol monomers: Synthesis, applications, and perspectives," *SusMat* 2 no.5 (2022):535–568. https://doi.org/10.1002/sus2.87.

21. J. Wang, Q. Liu, J. Yu, et al., "Synthesis and Characterization of Benzoxazine Resin Based on Furfurylamine," *Materials* 15, no. 23 (2022): 8364. https://doi.org/10.3390/ma15238364.

22. P. Thirukumaran, R. Sathiyamoorthi, A. Shakila Parveen, et al., "New benzoxazines from renewable resources for green composite applications," *Polymer Composites* 37, no. 2 (2016): 573–582. https://doi.org/10.1002/pc.23214.

23. C. Wang, C. Zhao, J. Sun, et al., "Synthesis and thermal properties of a bio-based polybenzoxazine with curing promoter," *Journal of Polymer Science Part A: Polymer Chemistry* 51, no. 9 (2013): 2016–2023. https://doi.org/10.1002/pola.26587.

24. N. K. Sini, J. Bijwe, and I. K. Varma, "Renewable benzoxazine monomer from Vanillin: Synthesis, characterization, and studies on curing behavior," *Journal of Polymer Science Part A: Polymer Chemistry* 52, no. 1 (2014): 7–11. https://doi.org/10.1002/pola.26981.

25. X. Liu, Z. Li, G. Zhan, Y. Wu, et al., "Bio-based benzoxazines based on sesamol: Synthesis and properties," *Journal of Polymer Science Part A: Polymer Chemistry* 136, no. 48 (2019) 48255. https://doi.org/10.1002/app.48255.

26. M. Yu 2022. “Structure-Processing-Property Relationships of Furanyl Benzoxazine Polymers Derived from Bio-based Feedstocks.” Theses and Dissertations, Drexel University. https://doi.org/10.17918/00001287

27. M. Chauby 2024. "Chemistry and Processing of Carbon/Carbon Composites from Furan-Based Polybenzoxazine Resins.” Theses and Dissertations, Rowan University. https://rdw.rowan.edu/etd/3279

28. B. Münzenberger, J. Heilemann, D. Strack, et al., “Phenolics of mycorrhizas and non-mycorrhizal roots of Norway spruce,” *Planta* 182 (1990): 142-148, https://doi.org/10.1007/BF00239996.

29. A. C. Ferrari, “Raman spectroscopy of graphene and graphite: Disorder, electron-phonon coupling, doping and nonadiabatic effects,” *Solid State Communications* 143, nos. 1-2 (2007): 47–57. https://doi.org/10.1016/j.ssc.2007.03.052.

30. K. Jurkiewicz, M. Pawlyta, and A. Burian, “Structure of Carbon Materials Explored by Local Transmission Electron Microscopy and Global Powder Diffraction Probes,” *C* 4, no. 4 (2018): 68. https://doi.org/10.3390/c4040068.

31. T. Ko, W. Kuo, and Y. Chang, “Microstructural changes of phenolic resin during pyrolysis,” *Journal of Applied Polymer Science* 81, no. 5 (2001): 1084–1089. https://doi.org/10.1002/app.1530.

32. Z. Q. Li, C. J. Lu, Z. P. Xia, et al., “X-ray diffraction patterns of graphite and turbostratic carbon,” *Carbon* 45, no. 8 (2007): 1686–1695. https://doi.org/10.1016/j.carbon.2007.03.038.

33. X. Wu, N. Langhof, W. Krenkel, et al., “Effect of pyrolysis temperature on the microstructure and capillary infiltration behavior of carbon/carbon composites,” *Ceramics International* 44, no. 14 (2018): 16325–16332. https://doi.org/10.1016/j.ceramint.2018.06.034.

34. Y. Lu, M. Li, Y. Zhang, et al., “Synthesis and curing kinetics of benzoxazine containing fluorene and furan groups,” *Thermochimica Acta* 515, nos. 1-2 (2011): 32–37. https://doi.org/10.1016/j.tca.2010.12.014.

35. U. Lopez de Vergara, M. Sarrionandia, K. Gondra K, et al., “Polymerization and curing kinetics of furan resins under conventional and microwave heating,” *Thermochimica Acta* 581, no. 10 (2014): 92–99. https://doi.org/10.1016/j.tca.2014.02.017.

36. J. Hacaloğlu, T. Uyar, and H. Ishida 2011. “Thermal Degradation Mechanisms of Polybenzoxazines.” in *Handbook of Benzoxazine Resins*, Edited by H. Ishida and T. Agag, Elsevier: ISBN 9780444537904.

37. R. G. Ackman, W. H. Brown, and G. F. Wright, “The Condensation of Methyl Ketones with Furan” *The Journal of Organic Chemistry* 20, no. 9 (1955): 1147-1158. https://doi.org/10.1021/jo01126a001

38. R. E. Beals and W. H. Brown, “The Condensation of 3-Pentanone with Furan,” *The Journal of Organic Chemistry* 21, no. 4 (1956): 447-448. https://doi.org/10.1021/jo01110a019

39. W. H. Brown and H. Sawatzky, “The Condensation of Furan and Sylvan with some Carbonyl Compounds,” *Canadian Journal of Chemistry* 34 (1956): 1147-1153. https://doi.org/10.1139/V56-150

40. W. H. Brown and W. N. French, “The Condensation of Furan with Carbonyl Compounds,” *Canadian Journal of Chemistry*. 36, no. 3 (1958): 537-542. https://doi.org/10.1139/v58-075

41. G. Savage 1993. *Carbon-Carbon Composites*. 1st Edition. Springer Dordrecht. ISBN 978-94-011-1586-5.

42. J. Schulte-Fischedick, S. Seiz, N. Lützenburger, et al., “The crack development on the micro- and mesoscopic scale during the pyrolysis of carbon fibre reinforced plastics to carbon/carbon composites,” *Composites Part A: Applied Science and Manufacturing* 38, no. 10 (2007): 2171–2181. https://doi.org/10.1016/j.compositesa.2007.06.013.

43. G. M. Jenkins and K. Kawamura, “Structure of Glassy Carbon,” *Nature* 231 (1971): 175–176. https://doi.org/10.1038/231175a0.

44. G. S. Rellick, "Carbon and graphite matrices in carbon-carbon composites: An overview of their formation, structure, and properties. Technical report,” (1992).

45. A. C. Ferrari, J. C. Meyer, V. Scardaci, et al., “Raman spectrum of graphene and graphene layers,” *Physical Review Letters* 97 (2006): 187401. https://doi.org/10.1103/PhysRevLett.97.187401.

46. L. M. Malard, M. A. Pimenta, G. Dresselhaus, et al., “Raman spectroscopy in graphene,” *Physics Reports* 473, nos. 5-6 (2009): 51–87. https://doi.org/10.1016/j.physrep.2009.02.003.

47. B. Manoj and A. G. Kunjomana, “Study of Stacking Structure of Amorphous Carbon by X-Ray Diffraction Technique,” *International Journal of Electrochemical Science* 7, no. 4 (2012): 3127–3134. https://doi.org/10.1016/S1452-3981(23)13940-X.

48. A. M. Molodets and A. A. Golyshev, “Structural Transformations of Amorphous Carbon (Glassy Carbon) at High Shock Pressures,” *Journal of Experimental and Theoretical Physics* 126 (2018): 772–778. https://doi.org/10.1134/S1063776118060079.

49. J. Nam and J. Seferis, “Initial polymer degradation as a process in the manufacture of carbon-carbon composites,” *Carbon* 30, no. 5 (1992): 751–761. https://doi.org/10.1016/0008-6223(92)90158-S.

50. W. Zaman, K. Li, S. Ikram, et al., “Morphology, thermal response and anti-ablation performance of 3D-four directional pitch-based carbon/carbon composites,” *Corrosion Science* 61 (2012): 134–142. https://doi.org/10.1016/j.corsci.2012.04.036.